Proceedings of 20th International Congress on Acoustics, ICA 2010

23-27 August 2010, Sydney, Australia

Measurement of sound-radiation from a torpedo-shaped structure subjected to an axial excitation

Wei Liu (1), Jie Pan (1) and David Matthews (2)

(1) The University of Western Australia, Crawley WA 6009, Australia
(2) DSTO, HMAS Stirling, Rockingham WA 69582, Australia

PACS: 43.40.RJ

ABSTRACT

This paper summarizes the first part of results of measured sound radiation from a torpedo-shaped structure under an axial excitation. The structure, built for this study, is two meters in length consisting of a cylindrical shell, a semi-spherical shell at one end and a conical shell at the other. Due to the boundary constrains imposed by the semi-sphere and the cone at the ends of the cylinder, the structure exhibits notable difference in its dynamic behaviour from that of a shear-diaphragm supported cylinder with close-ends. We studied the first 13 structural modes experimentally and then concentrated on the sound radiation from each of those modes in an anechoic chamber structure. Foundings from this experimental work may be used to verify and support the previous analytical and numerical prediction of underwater sound radiation from a submarine hull. They may also find a broader application in noise analysis and control of unmanned underwater vehicle and marine structures.

1. INTRODUCTION

Among various practical situations, understanding and control of sound radiation from underwater structures, such as submarines and unmanned survey vehicles, are challenging tasks. Structural borne sound from these structures poses risks to have them exposed to other sonar devices and to reduce the signal-to-noise ratio of the self sonar systems. Understanding of such structure-borne sound is important to its prediction, optimisation and control [1], which also provides guidance for the design, manufacturing, and operation of those structures.

Although the structure-borne sound has been intensely studied by many researchers for several decades [2], clear understanding of the principle, mechanism and property of sound radiation are still confined to a few simple geometries with ideal boundary conditions. When dealing with more practical structures, it becomes difficult to extend the theory, due to the complexity of their complicated geometries, boundary conditions and material distribution.

A typical submarine structure consists of a cylindrical shell with a hemispherical shell at one end and conical shell at the other end. The vibration of continuous shell structure is complicated due to the added complexity of curvature, as well as the sophisticated boundary conditions [3]. Different shell theories have been derived in the past and have been used without united agreement.

Particularly, for a torpedo-shaped structures, discontinuity in the structures have important impact on the vibrational energy flow between different parts of the structure [4, 5], which contributes to the complexity of structural response and then changes the patterns of sound radiation from the structure. Various forms of discontinuities may exist in the torpedo-shaped structures, such as the discontinued curvature at the joints between the spherical, conical and cylindrical shells. They will affect not only the propagation of the flexural wave, but also on the in-plane waves in the structure.

Furthermore, the effect of structure-fluid interaction on structural borne sound is a key issues which cannot be circumvented. Although many researchers have devoted to this topic and some progress has been made in the past decades [6], many of these studies were actually based on numerical solutions or analytical methods with some approximations, for which experimental validations are essential and crucial. Thus, it appears necessary to conduct reliable experimental studies in supporting these theoretical works.

However, either due to confidential reasons, or because of the prohibitively high cost of carrying experimental research on a real submarine, nearly no published literatures can be found concerning such experimental studies of sound radiation from a submarine type structure.

This study is specifically concentrated on the experimental investigation of sound radiation from a torpedo-shaped structure, both in the air and underwater. The structure is a simplification of a scaled submarine model. Attention has been focused on the case that the structure is subjected to axial excitation, since propeller induced axial vibration is recognized to be the major source for sound radiation from submarine at low frequencies [7, 8].

As the first part of this experimental study, this paper summarizes the results of the structure's vibrational response and sound radiation into the air from the first 13 structural modes. The experiments were carried out in an anechoic chamber. In the following sections, we first describe the

setup of the test rig and measurement system. Then experimental procedure and data analysis are described. Finally, we summarize and discuss the results.

2. SETUP OF TEST RIG

2.1 model description

The torpedo-shaped structure is shown in Figure1. In this model, the semi-spherical shell and the cone shell were added to the cylinder via screw connection. To simulate the axial excitation, a mechanical shaker was employed at the end of the conical shell to apply an axial force along the central axis of the structure, where special attention had been paid to guarantee the excitation is cantered and towards the axial direction as accurately as possible. Mass blocks were designed and placed inside of the structure to balance the buoyant force during underwater test, which also represent the mass loading of onboard equipments.

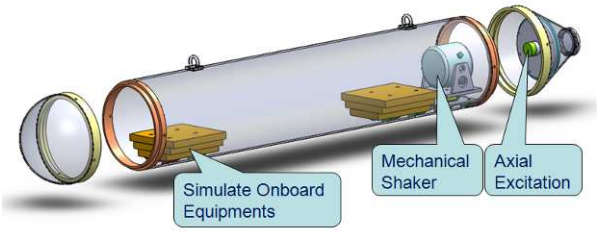

Figure 1 Experimental torpedo model

The model was geometrically scaled from the submarine model studied in [8]. The scale factor was 1:22.5. Table 1 lists the data of the model, where minor adjustment had been made for practical manufacturing.

Table 1 Experimental model data

Parameter	Value	Unit
Total mass	160	kg
Total length	2000	mm
Cylinder length	1500	mm
Radius	161.5	mm
Cylinder thickness	6	mm
Semi-sphere thickness	4	mm
Cone thickness	4	mm
Cone height	230	mm
Cone smaller radius	50	mm
Material	Carbon steel 1020	
Young's Modulus	200-210	GPa
Density	7872	kg/m^3
Working depth	40	m
Seal type	O-ring	

One of the key parts of the experimental rig design was to guarantee the experimental modal meets the requirements of a test 40 meters underwater. Proper design for seal, power supply, signal transmission and condition monitoring had been adopted to satisfy the requirements.

2.2 system setup

The setup for the experiments system is shown in the flow diagram in Figure 2.

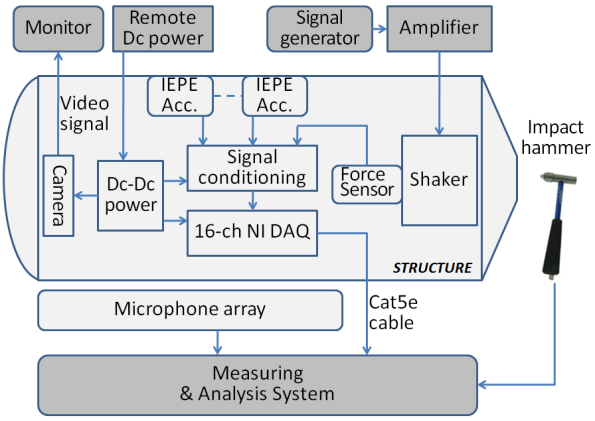

Figure 2 Experimental setup

The setup consists of three sections. The first section is the sound pressure measurement equipments, mainly the microphone array, which was outside the torpedo structure, and sited in the anechoic chamber. The second section is the structural response measurement equipments, sited inside the torpedo structure and include (a) IEPE accelerometers and signal conditioning modules (b) B&K force transducer (c) NI-DAQ (d) B&K electromagnetic shaker (e) Infrared Camera and (f) local DC-DC power supply.

The third section is for collecting signal, exciting the structure and monitoring the working condition inside the structure. The equipments for this section include (a) Signal generator (b) Power amplifier (c) Monitor (d) Remote AC-DC power supply (e) Measuring and analysis system and (f) Impact hammer.

In the experiments, sinusoidal signal was produced by the signal generator and amplified by the power amplifier before sending into the mechanical shaker. IEPE accelerometers were employed to measure the structural response, and the force transducer for measuring the excitation force applied by the shaker. To avoid using large bundles of long cables, all the analog signals were converted into digital signal before they were transmitted to the computer for analysis, which only requires one single Ethernet Cat5e cable. An infrared camera was utilised to monitor the condition of equipments inside the structure.

3. EXPERIMENTS

3.1 modal test

To study the dynamic behaviour of the torpedo-shaped structure, modal test had been carried out to identify the characteristic frequencies and corresponding mode shapes.

The three parts of the structure were assembled together, before the structure was freely suspended in the anechoic chamber to simulate the free-free boundary condition of a submarine. Figure 3 shows the grid of measuring points and the corresponding coordinates originated at the geometry centre of the structure. Along the circumferential direction of the structure, 12 points on each cross section were selected for vibration measurement. In total 25 cross sections were measured along the longitudinal (axial X) direction, with 6 on the semi-sphere, 14 on the cylinder and 5 on the cone. The cross sections were axially equal-spaced on the cylinder and the conical shell, and angularly equal-spaced on the semi spherical shell as well. The photo of the actual modal test is shown in Figure 4.

An impact hammer was used to apply impulse excitation to the structure along the axial direction. The measured

response was the acceleration in the normal direction to the shell surface (also referred as "radial" direction of the cylinder). Two sets of signals were collected for each measuring point, the structure acceleration and the impulse force. The Frequency Response Function (FRF) at each point was then calculated and saved for the synthesized modal analysis, where the resonance frequencies and modal shapes were identified.

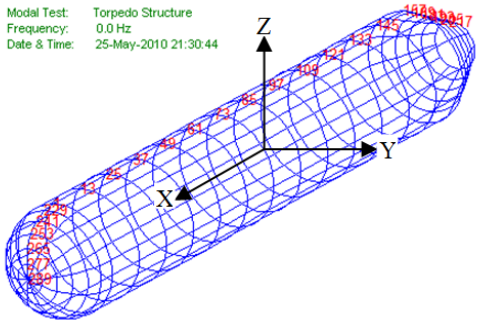

Figure 3 Measuring point arrangement for the modal testing

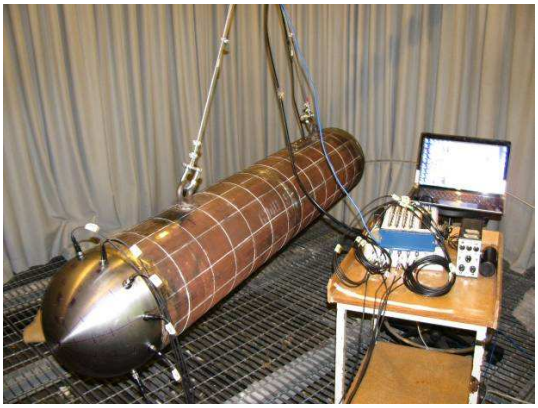

Figure 4 The testing rig for the modal testing

3.2 sound pressure measurement in anechoic chamber

After obtained the dynamic properties of the torpedo structure, the radiated sound pressure was measured in the anechoic chamber at each natural frequency of the structure. In this study, we focused on the directionality of the sound radiation from the first 13 modes, with natural frequencies ranging from 88Hz to 518Hz.

A sinusoidal signal at the natural frequency of the mode was sent to the shaker to excite the structure. The measurements of sound radiation were carried out on a semi-spherical surface above the torpedo structure, with the diameter of 4 meters, as shown in Figure 5. The origin of the surface coincided with the geometrical centre of the torpedo structure, which was also the origin of the XYZ coordinate defined in Figure 5. The XYZ coordinate is used in all the descriptions in the rest of this paper.

Due to the limitation of the space in the anechoic chamber, only the sound pressure on the upper semi-sphere of the surface was measured, which gives 145 points in total for each vibration mode. In each of the XY measurement circle (on the horizontal plane), pressure was measured at 24 points with an equal angular space of 15°. On each the vertical semi-circle (the 180° arc on each vertical plane), 13 measurement points were equally distributed in the angular space of 15°.

At each excitation frequency, the sound pressure signals at the 145 measuring points were collected by the microphone array. Figure 6 shows the photo of the actual sound pressure measurement.

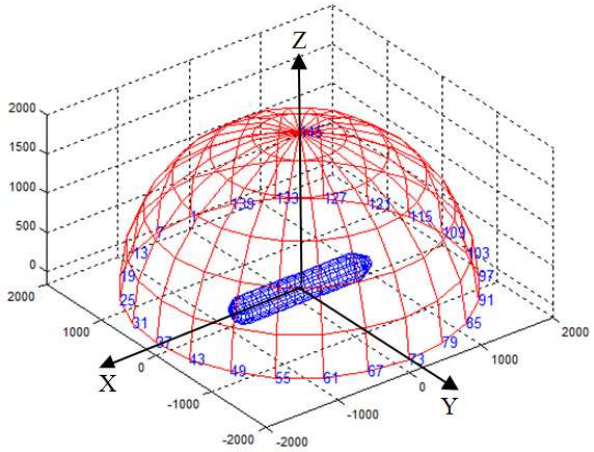

Figure 5 Measuring point arrangement of sound pressure

Figure 6 The actual rig of sound pressure measurement

3.3 data analysis

For the modal test, dual channel spectrum analysis was conducted for each measuring point to obtain the frequency response function (FRF). Due to the small structure damping, resonance peaks at characteristic frequencies are pretty clear. Corresponding to each frequency, the amplitude and phase information were extracted from the FRF functions for the calculation of modal shapes.

The sampling frequency for measuring the system response in the modal testing is 5000Hz. Attention was focused on the frequency range below 1000Hz, where the first 13 modes are located.

The sound pressure signals in time domain were measured through recording the analog output voltage of microphone array. Single channel spectrum analysis was then conducted to calculate the Power Spectrum Density (PSD) in the frequency domain for each measurement point.

4. RESULTS

4.1 modal test

To extract the modal characteristics of the structure, the measured accelerations at total 289 points are divided into three groups. The first group consists that from the 61 points on the semi-spherical shell, the second group consists of the results from the 168 points on the cylindrical shell and the last group corresponds to the 60 points on the conical shell. The spatial averaged FRF functions for each group are presented in Figures 7, 8 and 9. Together with mass distribution of the shells, they represent the spatial averaged vibration energy with respect to one unit force of excitation in the three shells of the structure. The plots start from 60Hz since there is no non-rigid body resonance peaks below this frequency.

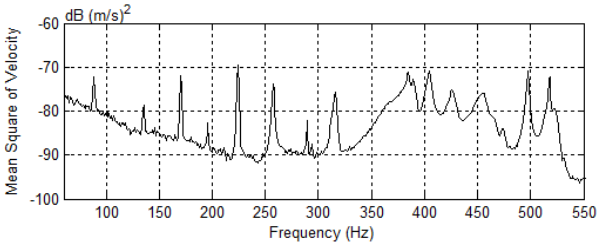

Figure 7 FRF plots of the semi-spherical shell

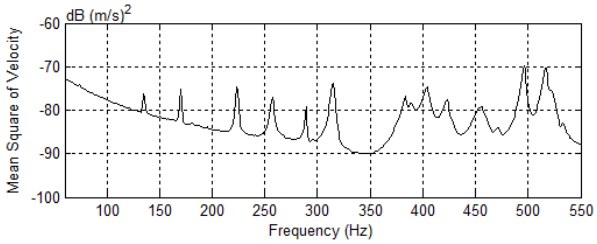

Figure 8 FRF plots of the cylindrical shell

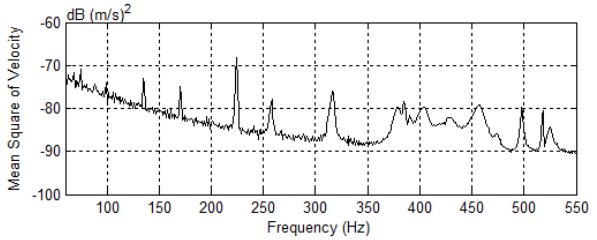

Figure 9 FRF plots of the conical shell

A) Modal Frequencies

From the spatial averaged energy response, the resonance peaks can be readily identified. Only very small differences were observed between some modal frequencies among the three sets of responses. After carefully examined those FRF, 13 resonant peaks were listed in Table 2, which were also used later as the excitation frequency for the sound pressure measurements.

Table 2 Frequencies for the first 13 peaks

No.	*Semi-spherical shell (Hz)*	*Cylindrical shell(Hz)*	*Conical Shell(Hz)*
1	88	-	-
2	136	135	135
3	170	170	170
4	224	224	224
5	257	258	257
6	290	289	-
7	316	315	316
8	384	383	378
9	405	405	405
10	425	425	425
11	455	455	455
12	498	496	498
13	518	518	518

B) Modal Shape at f=88Hz

The first peak observed on the semi-spherical shell is located at 88Hz, which is not observable on the other two shells. One might tempt to ignore this frequency; however, after carefully examining the corresponding modal shape, it was found that the vibration at this frequency actually represents an in-phase vibration mode of the spherical shell, pretty like the breathing mode of a circular cylindrical shell. The measured sound pressure (to be shown in section 4.2) from this mode also demonstrate that the semi-spherical shell is an efficient sound radiator at this frequency. Figure10 gives the modal shape of the semi-spherical shell and the distribution of radial vibration velocity.

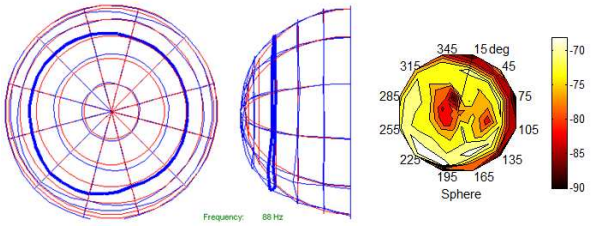

Figure10 FRF plots of the semi-spherical shell at 88Hz

C) Modal Shapes at f=136Hz~f=518Hz

Except for f=290Hz where there is no peak appears in the conical shell spectrum, all the peak frequencies are found in the three parts. The corresponding modal shape at each of these frequencies is complicated and requires some explanation.

Figure11-Figure22 presents the distribution of vibration velocity on the surface of the semi-sphere, the cylinder and the cone at each characteristic frequency. The velocity responses are in the direction normal to the shell surfaces. In each figure, the upper sub-plot shows the response of the cylinder. For the convenience of description, the cylinder has been expanded along the circumferential direction. From 0° to 360° is in the clockwise direction when looking from positive X (sphere end) to negative X (cone end) , with circumferential angle 0° sited on the positive Z-axis as defined in Figure 3. The lower-left and lower-right sub-plot show the velocity response of the sphere and the cone respectively, where the view direction is also from positive X (sphere end) to negative X (cone end) as defined in Figure 3.

The out-of-plane modes of the cylinder, the semi-sphere, the cone are summarised in Table 3, where n represents circumferential number and m axial node number. Among the modes obtained, circumferential number n=1, 2, 3 and axial node number m=0, 1, 2, 3 were observed. . It should be pointed out that the definition of number m here is different from Leissa [3], due to the difference of the boundary condition of the cylindrical shell. In [3], m refers to the number of half wavelength. The modal notation in the experimental results is just defined by the observation and not limited by the tradistional notation sequence for perfect cylinders.

Table 3 Node number of each modal shape

f (Hz)	*Cylinder*		*Sphere*	*Cone*	*Figure*
	n	***m***	***N***	***n***	
136	2	0	1	1, 2	Fig.11
170	2	1	1, 2	1	Fig.12
224	2	1	0, 1	1	Fig.13
257	2	1	1, 2	1, 2	Fig.14
290	2	0	1	1	Fig.15
316	2	0(1)	1, 2	1	Fig.16
384	2	3	1	1	Fig.17
405	1	3	1, 2	1, 2	Fig.18
425	2	2	1, 2	1, 2	Fig.19
455	1	3(2)	1, 2	1, 2	Fig.20
498	3	1	1, 2	1, 2	Fig.21
518	3	2	1	1, 2	Fig.22

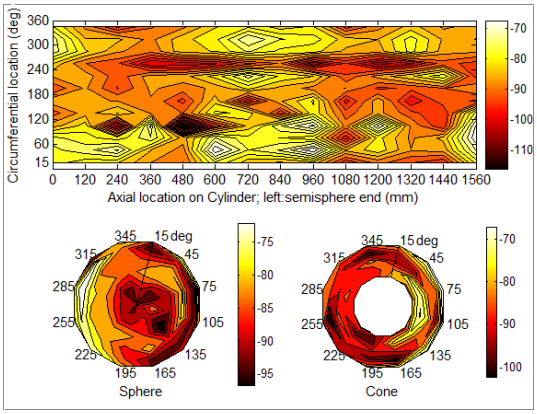

Figure11 Modal shape at ***f***=136Hz

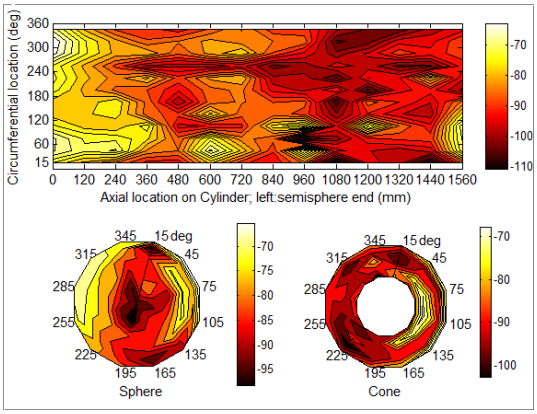

Figure12 Modal shape at ***f***=170Hz

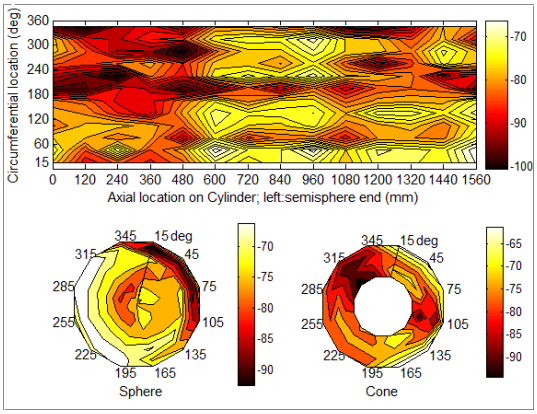

Figure13 Modal shape at ***f***=224Hz

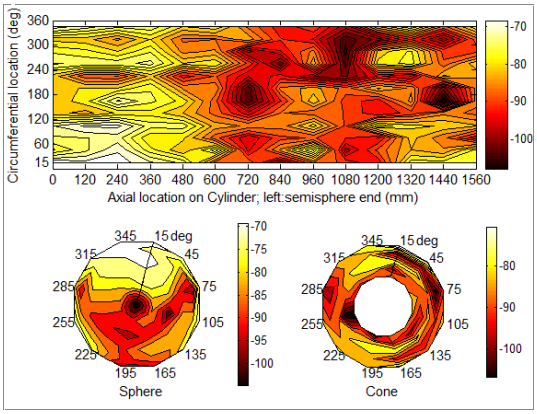

Figure14 Modal shape at ***f***=257Hz

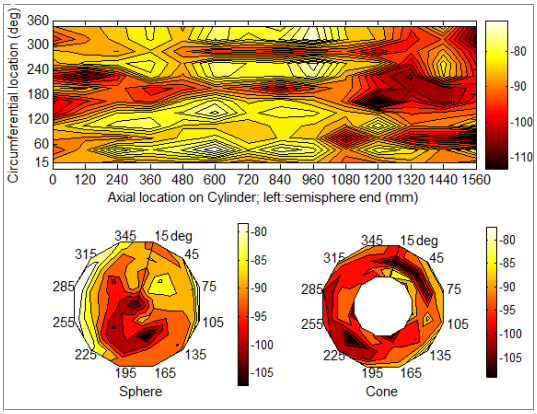

Figure15 Modal shape at ***f***=290Hz

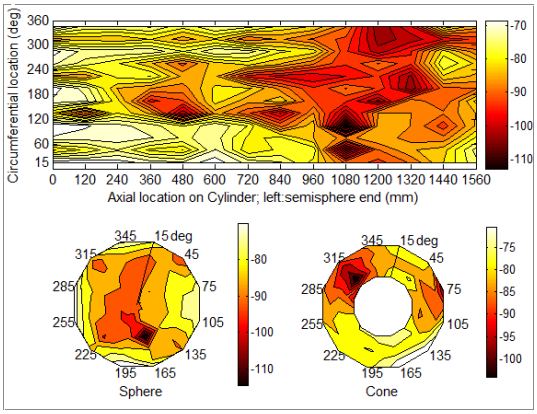

Figure16 Modal shape at ***f***=316Hz

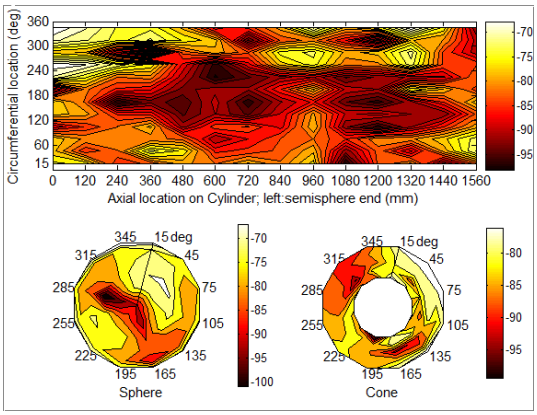

Figure17 Modal shape at ***f***=384Hz

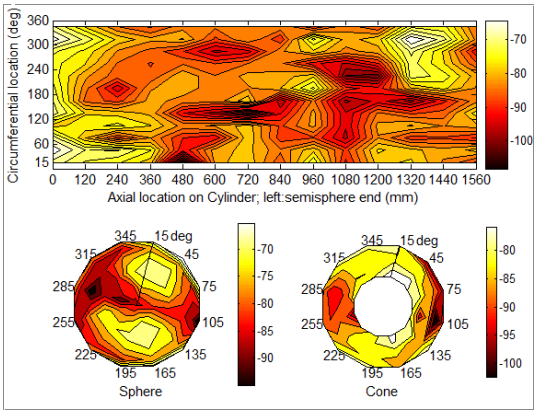

Figure18 Modal shape at ***f***=405Hz

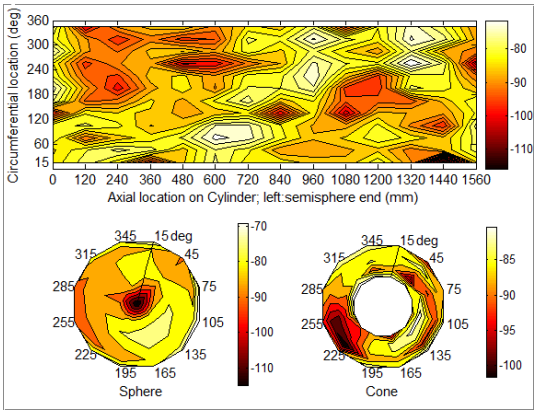

Figure19 Modal shape at ***f***=425Hz

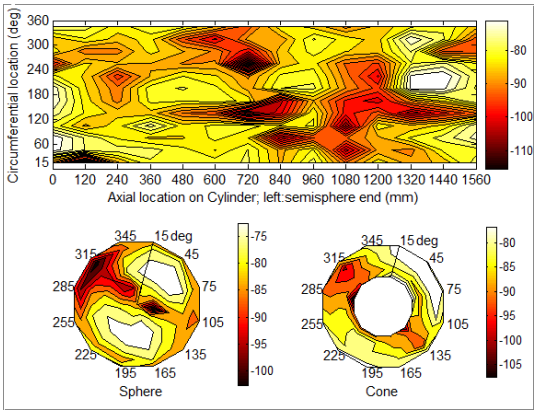

Figure20 Modal shape at ***f***=455Hz

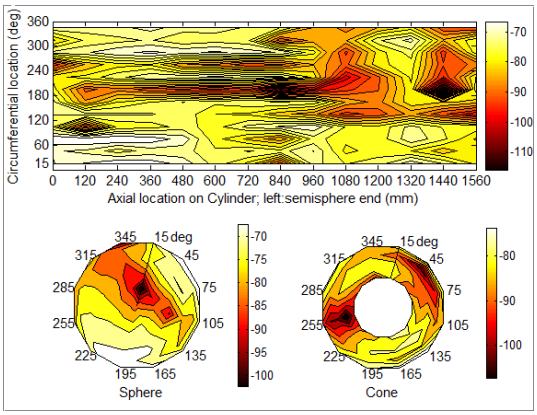

Figure21 Modal shape at ***f***=498Hz

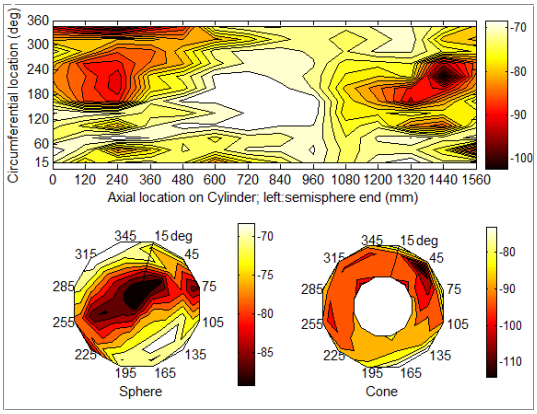

Figure22 Modal shape at ***f***=518Hz

The following observations and remakes are made from the above experimental results,

C.1) For those vibration modes with the same ***n*** and ***m*** number, it is difficult to determine which one is primarily radial vibration controlled, axial or torsional vibration controlled since the measurements were in the radial direction only.

C.2) Boundary conditions have a great effect on the modal shapes of the cylindrical shell. In Leissa [3], the boundary condition of the cylinder supported by shear diaphragms is assumed to be ***w***=***v***=0 at both ends, where ***w*** and ***v*** represent the displacements in radial and torsional directions respectively. However, for the torpedo-shaped structure, these boundary conditions no longer hold. Let's look at how the lowest frequency in each group with the same modal numbers (***m, n***) varies with ***m*** and for a fixed ***n***. In Leissa [3], these frequencies of the supported cylinder follow exact ascending order as ***m*** increases. For the torpedo-shaped structure, however, this may not be true. The lowest frequency of the (***n***=2, ***m***=3) mode (384Hz) is lower than the lowest frequency of the (***n***=2, ***m***=2) modes (425Hz), this observation can also be seen from Figure 23, which plots the lowest frequencies versus the axial number ***m.***

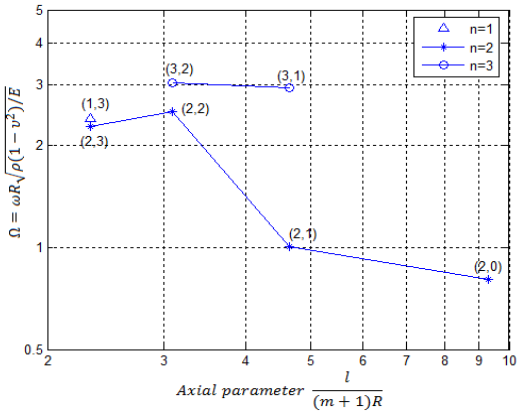

Figure23 The lowest frequencies at different modes (***n,m***)

The above results comparison is not about the whole structure, but about the cylinder, which is a closed end cylinder, while the SS boundary supported cylinder is also a closed end cylinder. From this point of view, the SS cylinder model is probably the closest model where detailed theoretical results are available and can be used as guidance of this experimental study for this type of cylinder.

C.3) Another interesting phenomenon is that the circumferential modes of the cylinder at each cross section

along the longitudinal direction are not consistent. The general trend is that circumferential distribution of each mode at the middle of the cylinder is different from that close to either the semi-spherical shell or the conical shell. Figure 24 shows an example at ***f***=518Hz. The sub-plot from left to right refer to the end section close to the semi-sphere, the middle section of the cylinder and the other end section close to the cone. The three cross section exhibit circumferential mode of number ***n***=2, 3, 2 respectively. Table 4 gives rise to the circumferential number of the three cross-sections at each frequency, where L is the length of the cylinder.

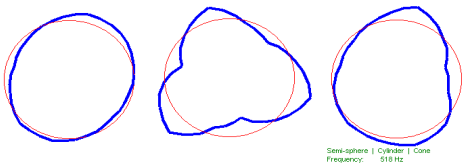

Figure 24 Circumferential modes at the end cross sections and the middle cross section of the cylinder

Table4 Circumferential number of three cross-sections

Frequency (Hz)	*Semi-sphere End(0-end)*	*Middle of the Cylinder*	*Cone End (L-end)*
136	2	2	1
170	2	2	1
224	2	2	1
257	2	2	2
290	2	2	2
316	2	2	1
384	2	2	1
405	2	1	2
425	2	2	1
455	2	1	1
498	2	3	2
518	2	3	2

It is obvious from table 4 that, at some frequencies, the circumferential modes at the two ends are different not only from the middle section, but also from each other.

C.4) Two modes have unclear ***m*** number, 0(1) at 316Hz and 3(2) at 455Hz. This means some of the longitudinal modal lines exhibit 0 node while the others exhibit 1 node at 316Hz; at 455Hz, some exhibit 2 node and the others have 3 nodes. This is probably related to the inconsistency of circumferential mode shapes at different cross sections of the cylinder mentioned above in **C.3**.

C.5) For the semi-spherical shell and the conical shell, circumferential number ***n***=1 can be observed at all frequencies, and circumferential number ***n***=2 can be observed at most of the frequencies.

C.6) The further study will investigate the effect of the the shaker's reaction on the structure. However, the comparions between the impact hammer test result and that by using the shaker showed that the reaction force will not significantly affect the structure's modal characteristics.

4.2 sound pressure measurement

For each frequency and corresponding modal shape listed in section 4.1, the radiated sound pressures at the corresponding modal frequencies were measured on the upper semi-spherical surface with a diameter of 4 meters.

A) Maximum sound pressure at each mode

Table 5 lists the maximum sound pressure value for each mode. The input driving voltages of the shaker inside the torpedo were kept as the same for all measurements.

Table 5 Maximum sound pressure at each frequency

Frequency (Hz)	*Vibration Modes (**n,m**)*	*Maximum Sound Pressure (dB)*	*Figure Num.*
88	-	55	Fig. 25
136	(2,0)	56	Fig. 26
170	(2,1)	50	Fig. 29
224	(2,1)	58	Fig. 30
257	(2,1)	60	Fig. 31
290	(2,0)	60	Fig. 27
316	(2,0(1))	60	Fig. 28
384	(2,3)	64	Fig. 33
405	(1,3)	76	Fig. 34
425	(2,2)	68	Fig. 32
455	(1,3(2))	77	Fig. 35
498	(3,1)	63	Fig. 36
518	(3,2)	64	Fig. 37

B) Sound pressure distribution and directionality

In the following summary of sound distribution, the results at different modes are grouped together in accordance with their modal number (***n, m***), i.e., the modes with same (***n, m***) number are put together for comparison.

Due to the space limitation of this paper, only one 3D overall distribution and two 2D directivity of sound pressure are presented for each mode, which are represented by different subplot in each figure.

Upper subplot: top view (from Z look down into XY plane) of overall 3D sound distribution on the whole measuring surface, each point has its latitude in Z direction.

Middle subplot: directivity of sound pressure in the XY plane.

Lower subplot: directivity of sound pressure in the XZ plane.

B.1) ***f***=88Hz

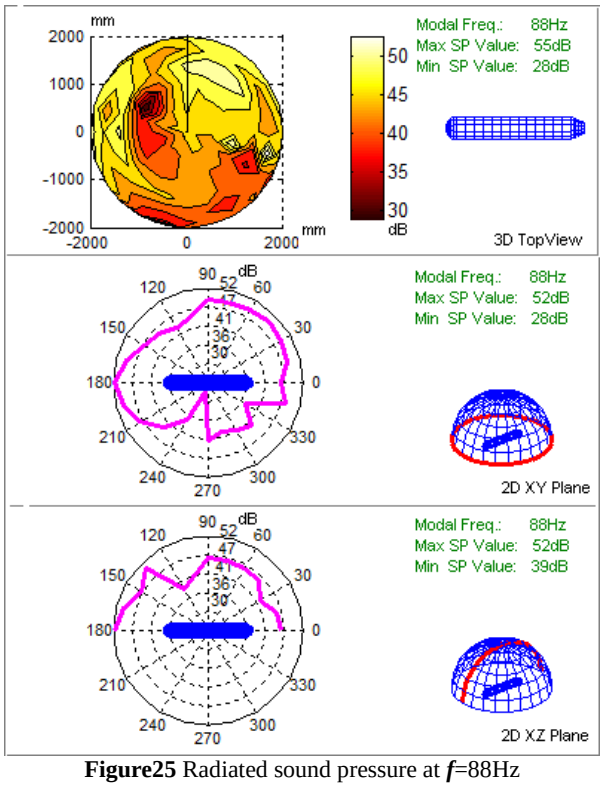

Figure25 Radiated sound pressure at ***f***=88Hz

B.2) Modes (***n***=2, ***m***=0), ***f***=136Hz, 290Hz, 316Hz

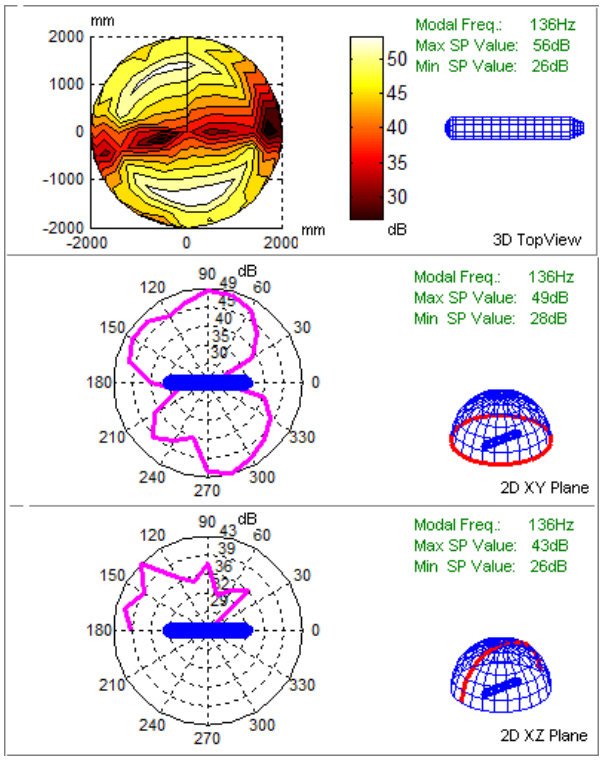

Figure26 Radiated sound pressure at ***f***=136Hz (***n***=2, ***m***=0)

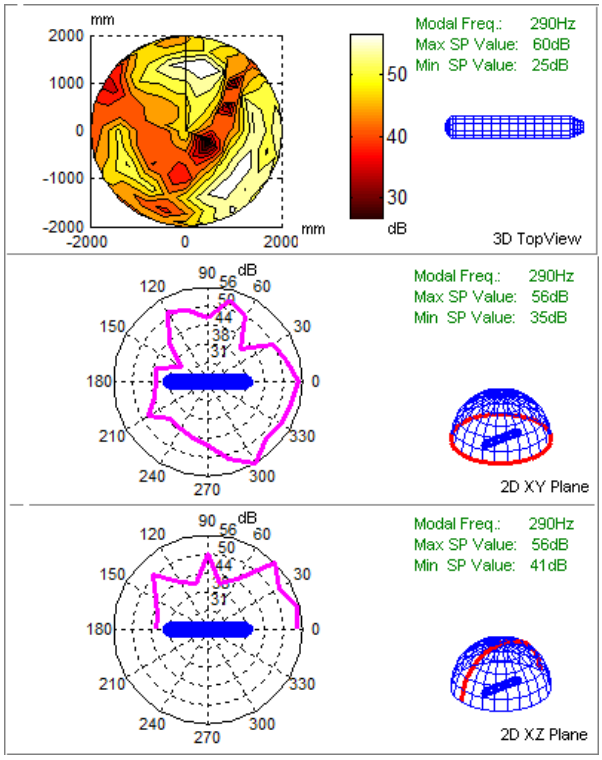

Figure27 Radiated sound pressure at ***f***=290Hz (***n***=2, ***m***=0)

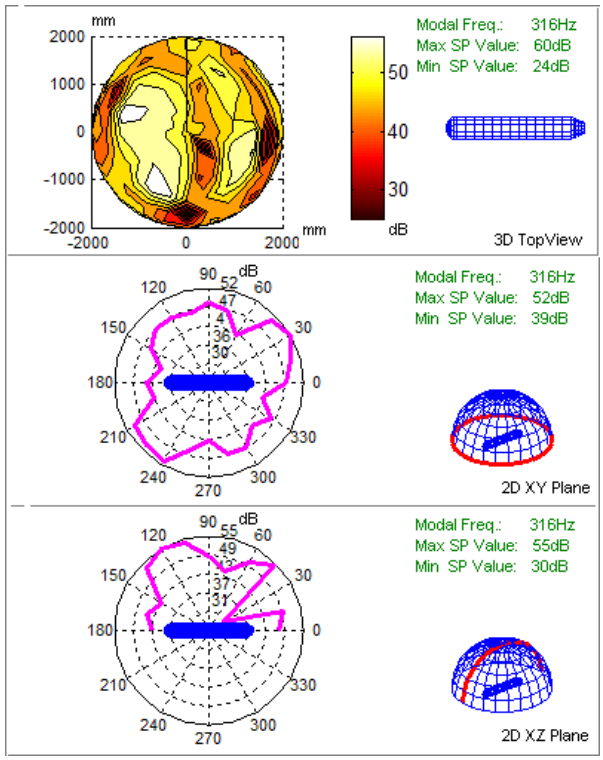

Figure28 Radiated sound pressure at ***f***=316Hz (***n***=2, ***m***=0)

B.3) Modes (***n***=2, ***m***=1), ***f***=170Hz, 224Hz, 257Hz

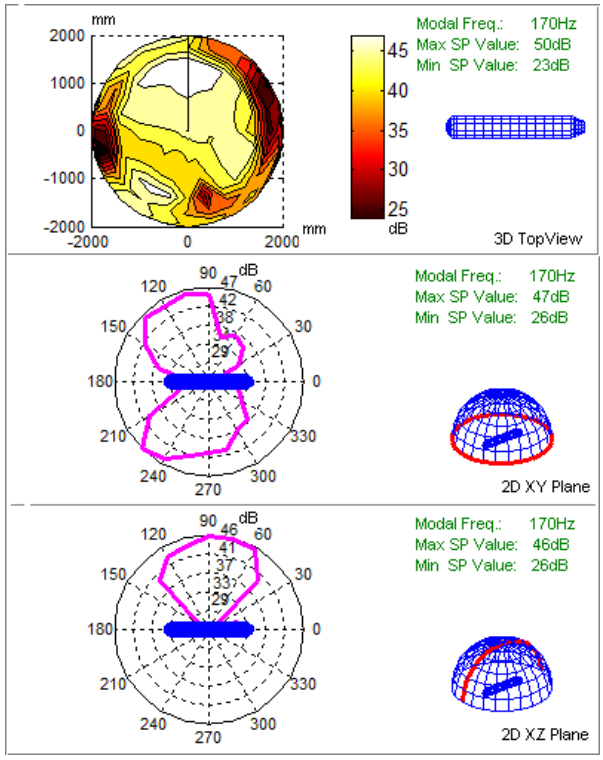

Figure29 Radiated sound pressure at ***f***=170Hz (***n***=2, ***m***=1)

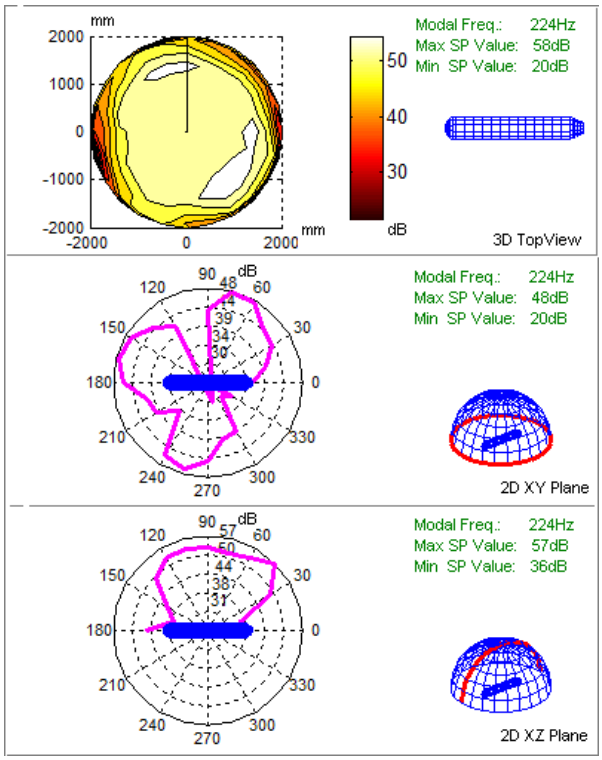

Figure30 Radiated sound pressure at ***f***=224Hz (***n***=2, ***m***=1)

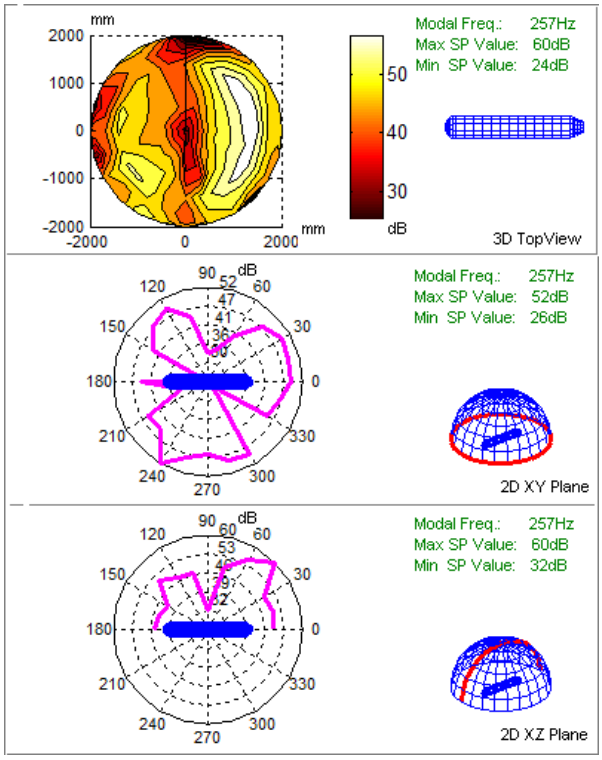

Figure31 Radiated sound pressure at ***f***=257Hz (***n***=2, ***m***=1)

B.4) Modes (***n***=2, ***m***=2), ***f***=425Hz

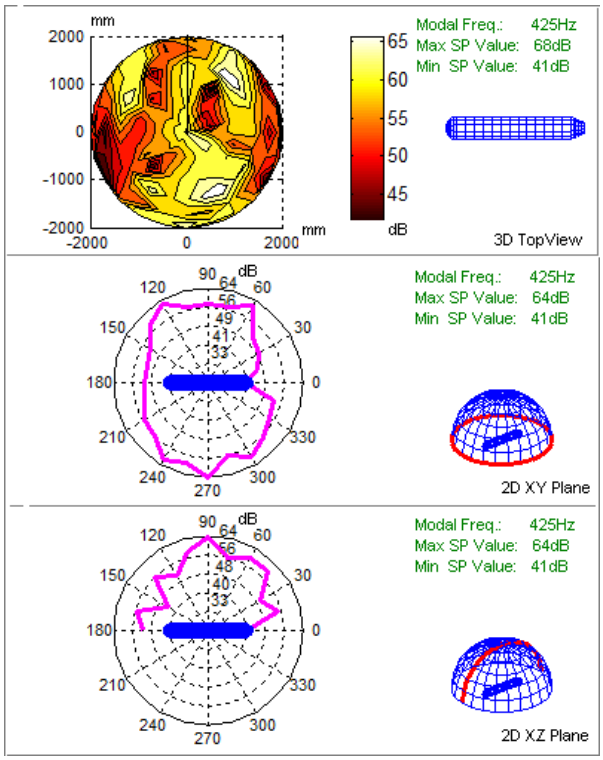

Figure32 Radiated sound pressure at ***f***=425Hz (***n***=2, ***m***=2)

B.5) Modes (***n***=2, ***m***=3), ***f***=384Hz

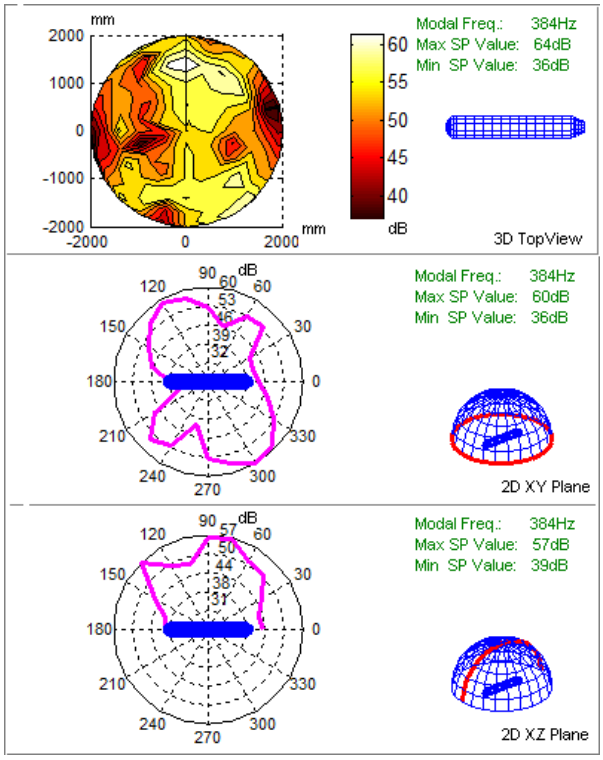

Figure33 Radiated sound pressure at ***f***=384Hz (***n***=2, ***m***=3)

B.6) Modes (***n***=1, ***m***=3(2)), ***f***=405Hz, 455Hz

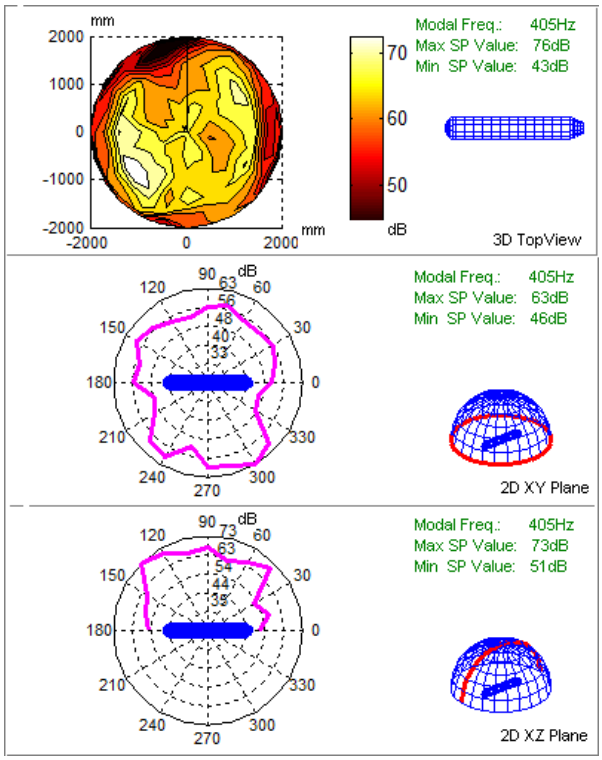

Figure34 Radiated sound pressure at ***f***=405Hz (***n***=1, ***m***=3)

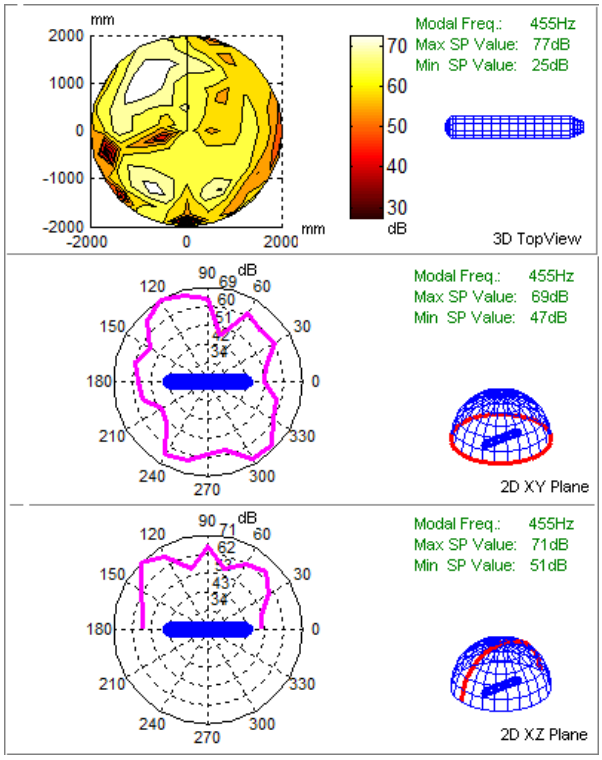

Figure35 Radiated sound pressure at ***f***=455Hz (***n***=1, ***m***=3(2))

B.7) Modes (***n***=3, ***m***=1), ***f***=498Hz

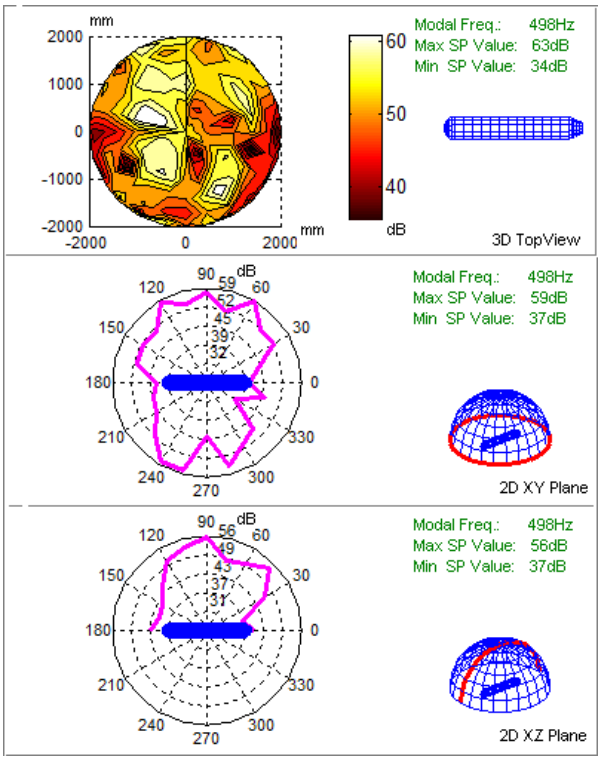

Figure36 Radiated sound pressure at ***f***=498Hz (***n***=3, ***m***=1)

B.8) Modes (***n***=3, ***m***=2), ***f***=518Hz

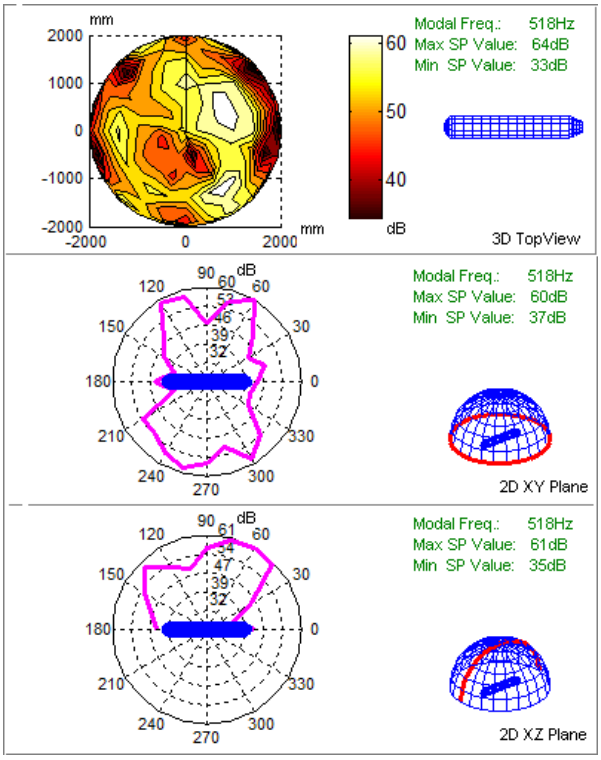

Figure37 Radiated sound pressure at ***f***=518Hz (***n***=3, ***m***=2)

C) Observations and Remarks

The following observations and remarks are offered.

C.1) Table 5 shows that the two modes with circumferential number ***n***=1 has the two largest sound pressure value. They are ***f***=405Hz with (***n***=1, ***m***=3) and ***f***=455Hz (***n***=1, ***m***=3(2)). The maximum sound pressure roughly increase for the first several modes and reach the largest value at ***f***=455Hz (***n***=1, ***m***=3(2)), then decrease afterwards.

C.2) The maximum sound pressure locations are found to be normally in the direction of 45-60 degrees relative to the XY plane, shown by the upper sub plot in each figure.

C.3) For the same circumferential number ***n***, there is no clear trend linking the sound pressure and axial node number ***m***, the same happens to different number ***n*** with the same number ***m***. For the same modal number pair (***n***, ***m***), the maximum sound pressure generally increase along the frequency, which can be seen with the three modes of (***n***=2, ***m***=0), the three modes of (***n***=2, ***m***=1) and the two modes of (***n***=1, ***m***=3).

C.4) In most modes, due to the asymmetric boundary conditions imposed by the semi-sphere and the cone, the sound radiations from the fore end (semi-spherical end) and the rear end (conical end) of the torpedo structure are not symmetric, i.e., the sound radiation is asymmetric about the YZ plane defined in Figure 5. This conclusion can be obtained from the lower sub-plot of each figure. There is also no dominating trend of which end has greater sound radiation. At some modes, the fore end radiation is greater while at other modes the rear end dominates. This observation is recorded as the property of "Fore-Rear symmetric about YZ" in table6.

C.5) One interesting observation from examining the middle sub-plot of each figure is that for some of the modes, the sound radiation of the left side and the right side is not symmetric regarding to the central vertical plane (XZ plane defined in Figure 5), although the structure is designed to be symmetric about this plane. One possible factor could be the deviation of the manufacturing from the design, which leads to the slight asymmetry of the actual structure. However, not all modes are subjected to the influence of geometry asymmetry; some modes still exhibit symmetric or roughly symmetric properties. The results are recorded as the property of "Left-Right symmetric about XZ" in table6.

Table 6 Symmetry property of sound radiation

Frequency (Hz)	*Vibration Modes* ***(n,m)***	*Fore-Rear Symmetric About YZ*	*Left-Right Symmetric About XZ*
88	-	Fore > Rear	No
136	(2,0)	Fore > Rear	Roughly
170	(2,1)	Yes	Yes
224	(2,1)	Fore < Rear	No
257	(2,1)	Fore < Rear	Roughly
290	(2,0)	Fore < Rear	No
316	(2,0(1))	Fore > Rear	No
384	(2,3)	Fore > Rear	No
405	(1,3)	Roughly	Roughly
425	(2,2)	Yes	Yes
455	(1,3(2))	Yes	Yes
498	(3,1)	Fore < Rear	Roughly
518	(3,2)	Fore < Rear	Yes

C.6) For those modes with the same (***n***, ***m)*** number pair, the directivity of sound radiation could be noticeably different from each other, which can be seen from the two modes with (***n***=2, ***m***=3), the three modes with (***n***=2, ***m***=0), as well as the three modes with (***n***=2, ***m***=1).

C.7) At ***f***=88Hz, due to the in-plane vibration modes observed in section 4.1, the semi-spherical shell is anticipated to be more efficient in sound radiation under this frequency. Indeed through examining the sound pressure at the location in front of the semi-sphere, It is found that the radiated sound pressure at ***f***=88Hz is one of the largest among all the other frequencies, only slightly smaller than the two modes with ***n***=1) at ***f***=405Hz and 455Hz.

5. CONCLUSIONS

This paper summarizes the experimental results of vibration and sound radiation of a torpedo-shaped structure subjected to axial excitation. It has been shown that the structure's dynamic behaviour is noticeably different from that of a typical diaphragm supported close-end cylinder. It was observed that due to the impact of the boundary conditions imposed by the spherical shell and the conical shell, the lowest natural frequency is not increase along with the axial node number ***m*** for the same circumferential number ***n***. It was also noticed that there is normally no consistent modal shape along the cylinder, the ends and the middle section could exhibits different circumferential mode shapes. As the consequence, the axial node number ***m*** at some frequencies is not clear.

Regarding to the sound radiation at each mode, the two modes with circumferential number ***n***=1 have the two largest sound pressure among all the modes. The sound radiation of the sphere is efficient with the presence of in-phase modes on it. The maximum sound pressure roughly increase at lower modes, and decrease with the last 3 modes; nevertheless, there is no general trend relating the maximum sound pressure with modes number pair (***n, m***). For each mode, the maximum pressure often occurred in the direction of 45-60 degrees relative to the XY plane. The sound distribution is not fore-end to rear-end symmetric due to the asymmetry of the torpedo structure in the axial direction. Besides, it is also left-side to right-side asymmetric at some modes.

The effect of the heavy fluid loading on the structural vibration and sound radiation will be the subject of a following up experiment.

Acknowledgement: The supports of the IPRS, UPA and SAMAHA scholarship from the Australian Government and the University of Western Australia to the first author are greatly appreciated.

REFERENCES

1 X. Pan, Y. Tso and R. Juniper “Active control of radiated pressure of a submarine hull” s.l.: Elsevier, 2007, Vol. 311, 224–242 (2008)
2 L. Cremer, and M. Heckl, Structure-Borne Sound, 2nd edn (trans. E.E. Ungar) (Springer-Verlag, Berlin, 1988)
3 A. W. Leissa, Vibration of Shells (American Institute of Physics, Woodbury, New York, 1993)
4 C. R. Fuller, “The effects of wall discontinuities on the propagation of flexural waves in cylindrical shells”, Journal of Sound and Vibration 75(2), 207-228, (1981)
5 A. Harari, “Wave propagation in a cylindrical shell with joint”, Shock and Vibration Bulletin ***48***, 53-61, (1978)
6 D. G. Crighton, “Fluid loading: the interaction between sound and vibration”, Rayleigh medal lecture, University of Cambridge, (1988)
7 M. Caresta, N.Kessissoglou, “Signature of a submarine hull under harmonic excitation”, Cairns: ICSV14, (2007)
8 S. Merz, N. Kessissoglou, and R. Kinns, “Excitation of a submarine hull by propeller forces”, Cairns: ICSV14, (2007)